

Space-time calibration of wind speed forecasts from regional climate models

Luiz E. S. Gomes¹ Thaís C. O. Fonseca^{1,2*}
 Kelly C. M. Gonçalves¹ Ramiro Ruiz-Cárdenas³

¹Federal University of Rio de Janeiro, Brazil

²University of Warwick, UK

³Consultant, Belo Horizonte, Brazil

Abstract

Numerical weather predictions (NWP) are systematically subject to errors due to the deterministic solutions used by numerical models to simulate the atmosphere. Statistical postprocessing techniques are widely used nowadays for NWP calibration. However, time-varying bias is usually not accommodated by such models. Its calibration performance is also sensitive to the temporal window used for training. This paper proposes space-time models that extend the main statistical postprocessing approaches to calibrate NWP model outputs. Trans-Gaussian random fields are considered to account for meteorological variables with asymmetric behavior. Data augmentation is used to account for censoring in the response variable. The benefits of the proposed extensions are illustrated through the calibration of hourly 10 m wind speed forecasts in Southeastern Brazil coming from the Eta model.

Keywords: Data augmentation; Eta model; Spatiotemporal dynamic linear models; Statistical postprocessing; Wind speed forecasting

1 Introduction

Numerical weather predictions (NWP) are often based on mathematical models which make deterministic predictions from current atmospheric conditions. Such

*Address for correspondence: Thaís C. O. Fonseca, Department of Statistics, University of Warwick, Coventry, CV4 7AL, UK. E-mail: Thais.Oliveira-Da-Fonseca@warwick.ac.uk

models rely on complex systems of differential equations that do not have an analytical solution. Therefore, numerical integration is used to simulate physical, dynamic, and thermodynamic processes of the atmosphere depending on its current state. From this initial solution, it is possible to solve the system for any future time of interest (Krishnamurti, 1995).

These numerical systems are solved in a discrete grid which means that the model assumes uniform predictions for any point in the region belonging to a given cell of the grid. In particular, forecasts at each grid cell are based on average data in its region (e.g. average elevation and predominant vegetation). Note that, under these assumptions, the representativeness of predictions in cells with, for example, complex orography, dense vegetation or presence of water bodies, becomes deficient due to differences between the actual characteristics of the surface and the homogenization made by the model. Therefore, outputs from NWP models may not be representative at specific locations (Chou et al., 2007), thus producing systematic errors.

Meteorological phenomena are often not well described by a single numerical prediction. As an alternative, ensembles of forecasts, i.e, groups of outputs coming from multiple runs of either, the same or several models under varying initial conditions and model physics, are considered to allow for some sort of uncertainty quantification. The ensembles might be interpreted as a Monte Carlo experiment aiming to produce a range of future states of the atmosphere from different initial conditions (Epstein, 1969). Besides, the simulation of scenarios might indicate extreme events which would not be identified by just one run of the numerical model (Grimit and Mass, 2007). However, according to Gneiting et al. (2005), ensemble forecasts are often under dispersive, i.e., the ensemble spread is too narrow to account for all the uncertainty. As a solution, calibration is often considered to correct these error patterns.

Statistical postprocessing techniques have been widely used in recent years to minimize the above limitations of numerical models and to enhance both, the reliability and statistical consistency of numerical weather predictions. A sort of methods is nowadays available for the statistical calibration of ensemble forecasts. Recent reviews on this subject can be found in Li et al. (2017) and Vannitsem et al. (2018). The pioneer postprocessing technique in this context was the Model Output Statistics (MOS, Glahn and Lowry, 1972) which considers a multiple linear regression relating the responses (e.g. observed wind) to the set of ensemble members, assuming constant variance. Several extensions of this precursor method were proposed such as Updatable MOS (UMOS, Wilson and Vallée, 2002) which varies the size of the training period, MOC (Mao et al., 1999) which models directly the prediction error, and the generalized MOS (e.g. Piani et al., 2010) which consider generalized linear models instead of Gaussian distributions for the response vector.

An extension of MOS technique known as Ensemble MOS (EMOS, [Gneiting et al., 2005](#)), allows for a spread-skill relationship between the dispersion of ensemble members, and the response variance ([Whitaker and Loughe, 1998](#)). In the context of spatial calibration, the Geostatistical Output Perturbation (GOP, [Gel et al., 2004](#)) allows spatial dependence resulting in calibrated weather fields for a fixed temporal horizon. Moreover, the Spatial EMOS (SEMOS, [Feldmann et al., 2015](#)) combines the EMOS and GOP techniques.

Estimation of parameters in statistical postprocessing usually occurs in a subset of the data, called as a training period, defined through a moving time window that accounts for the effect of both, past observations and numerical predictions. If the training period is reasonably long it becomes easier to estimate the uncertainty in predictions ([Gneiting, 2014](#)). However, longer training periods may introduce distortions in the calibration due to seasonal effects. This challenging trade-off suggests that the window size must be tailored for the specific application to achieve better results. To illustrate, [Raftery et al. \(2005\)](#) analyzed the effects of the training window size on the uncertainty estimation of parameters in the calibration of temperature and sea level pressure predictions coming from the same numerical model. The author reported gains with the use of a time window as large as 25 days for both case studies and highlighted the need for an automatic way of choosing the length of the training period.

The above shortcomings of current statistical postprocessing approaches could be addressed by the incorporation of statistical techniques such as spatially structured calibration models. This approach may be useful in correcting NWP errors in regions where numerical models have smoothed important characteristics of the terrain, while the Kalman filter ([Kalman, 1960](#)) and Bayesian dynamical models ([West and Harrison, 1997](#)) are natural alternatives to account for seasonality and temporal dynamics of bias in postprocessing models.

This paper proposes a unifying approach to statistical postprocessing by accounting for temporal dependencies. It overcomes the need for large time windows in the definition of training sets. It is also able to accommodate spatial features from the terrain, as well as fairly skew and censoring behavior of the response, which might be essential for prediction and uncertainty quantification of certain variables like wind speed. The proposal is inspired in current postprocessing approaches, which are extended based on both, spatial dynamic linear models and data augmentation techniques. An optimized Markov chain Monte Carlo (MCMC) scheme based on robust adaptive Metropolis ([Vihola, 2012](#)) is used to perform efficient statistical inference and prediction.

The primary motivation of this study is the calibration of 10 meters wind speed forecasts since that meteorological variable presents some particular features that might not be properly addressed by the usual postprocessing techniques. Ac-

cording to [Ailliot et al. \(2006\)](#), some of these features include: intermittent atmospheric regimes with predominance of a certain direction of wind in certain regions; spatial and temporal correlation; non-Gaussianity; non-stationarity; conditional heteroscedasticity, i.e., the variance of the wind speed changes frequently in time; seasonal annual and diurnal components due to the effects of the sun and seasons; and possible trends.

Additionally, NWP models usually restrict wind speed forecasts to positive values. Therefore, zero wind speed predictions are not explicitly allowed. It leads to an overestimation of forecasts in the case of lower wind speeds (including zero), which are commonly observed in most regions, as illustrated in our application.

The remainder of this article is organized as follows. Section 2 presents the wind speed data which motivates our proposed modeling approach. Section 3 briefly describes the main postprocessing approaches used to calibrate numerical weather forecasts; section 3.2 presents the proposed extensions to enhance current postprocessing techniques and describes the inference procedure. Performance of the proposed extensions is evaluated and compared with current approaches in section 4. The article concludes with a discussion in Section 5.

2 Wind speed data for the state of Minas Gerais

The main motivation for the proposed models presented in this paper is the calibration of wind speed forecasts generated by the Eta regional climate model for the state of Minas Gerais, Brazil. The state of Minas Gerais, located in the Southeast region of Brazil, is entirely formed by plateaus and presents a rugged relief, ranging from 100 to 2800 meters above sea level, which give to the state exceptional water resources. The predominant vegetation, known as *Cerrado*, is characterized by large variations in the landscape between the rainy and dry seasons. It results in a seasonal influence of the surface roughness on the displacement of the winds, that are more intense during winter and spring seasons. The climate in Minas Gerais varies from hot semi-arid to humid mesothermal. Rainfall distribution is nonuniform in the state, with the north presenting long periods of drought and the highest temperatures, while the southern region (high elevation areas) concentrates the highest total annual rainfall ([Amarante et al., 2010](#)).

Two sources of hourly 10 m wind speed data for the region of interest, covering the two years from 1 October 2015 to 30 September 2017, were used in this application: ground measurements and numerical forecasts. The measurement data are recorded across an irregular network of weather stations from the Brazilian National Institute of Meteorology (INMET), available at <<http://www.inmet.gov.br>>. A set of 68 stations from this network, spread over Minas Gerais and its surroundings were selected with the requirement of at least 70% of data availability.

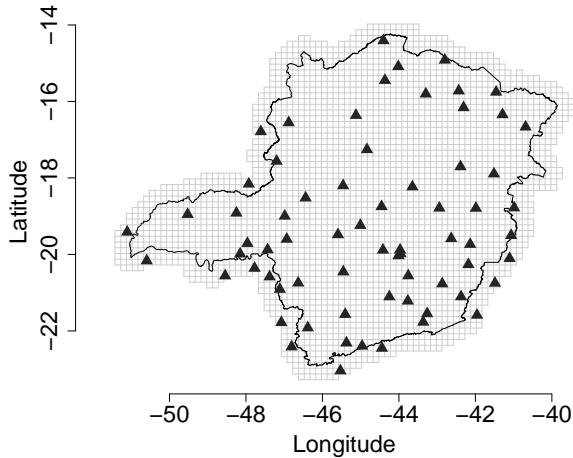


Figure 1: Map of Minas Gerais showing the location of the 68 weather stations (solid triangles). The solid lines represent the regular grid of the Eta regional climate model model with resolution of 15 km.

In this data, distances in space range from 7.9 to 1145 km and elevation of stations vary between 60 to 1359 m. The numerical accuracy of the data is one decimal place.

Numerical forecasts are generated by the Eta model (Mesinger et al., 1988; Black, 1994). It is a regional climate model run at the Center for Weather Forecasting and Climate Studies (CPTEC). Its extent covers most of South America and Central America. The model is issued twice a day at 0000 UTC and 1200 UTC. This study used hourly Eta model outputs from the run initialized at 1200 UTC with a horizontal resolution of 15 km, 50 vertical layers and a lead time of up to 264 hours (11 days). This lead time allows for up to 10 different wind speed forecasts for each hour, coming from the daily runs of the model. These groups of forecasts composed our ensembles in this application. This was because just one version of the model is issued at each running time. Hence, ensembles of forecasts for several numerical models were not available. Figure 1 presents the distribution of selected stations in the region of interest as well as the discrete grid of the numerical model.

Gridded forecasts were bilinearly interpolated to the locations of the 68 stations, to form the data set with hourly 10 m wind speed forecasts for calibration at these locations. Gel et al. (2004) argues that more complex interpolation methods can be used but it is unlikely that there will be considerable gains if the grid is considerably fine.

To illustrate the local characteristics of wind speed, Figure 2 presents some histograms with the wind speed distribution over the seasons at the following selected stations: Viçosa, Muriaé, and Pampulha (Belo Horizonte). The histograms

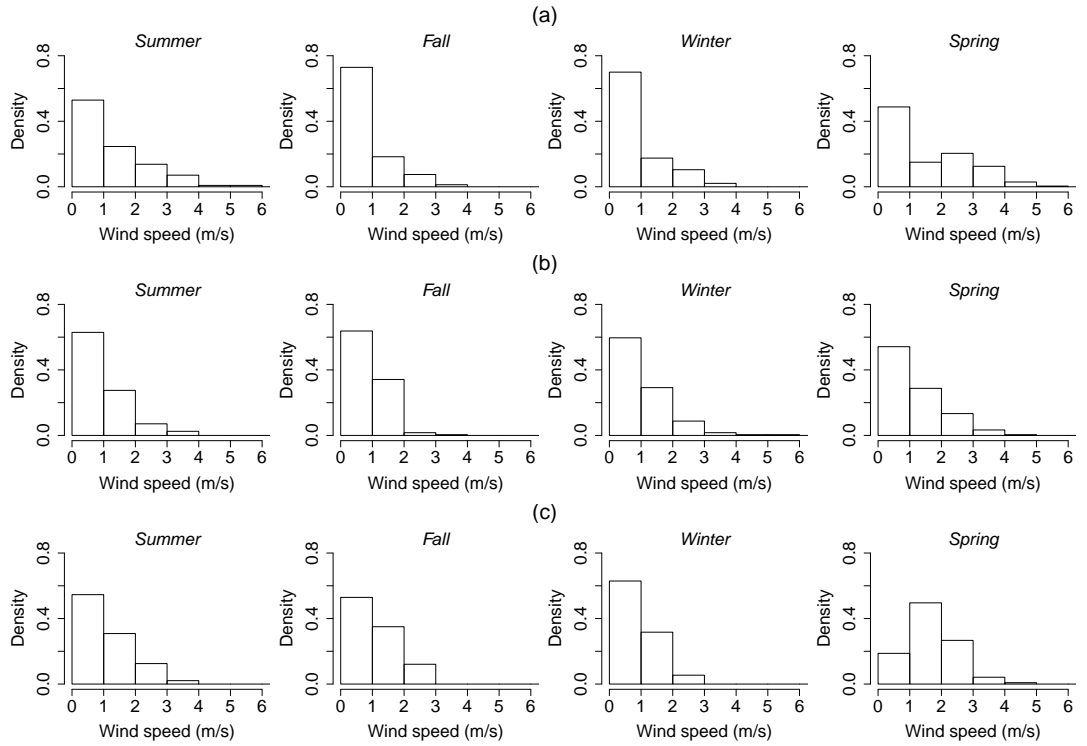


Figure 2: Histograms of observed wind speed at 10 meters over the seasons from 1 October 2015 to 30 September 2017 at (a) Viçosa, (b) Muriaé, and (c) Pampulha (Belo Horizonte) weather stations.

clearly show an asymmetric distribution with a frequent point mass at zero. In general lower wind speeds are recorded during the fall and summer and this pattern extends to the vast majority of available weather stations on the dataset. Particularly, the wind speed recorded during the spring has the highest threshold and the smallest point mass at zero. This wind regime is even more evident at the Pampulha (Belo Horizonte) weather station, as illustrated in Figure 2(c). These specific aspects in wind speed distribution motivate the space-time postprocessing models proposed in this paper, beside the need to consider the left censoring and data transformation.

3 Statistical postprocessing models

As follows the main postprocessing models used in the probabilistic calibration of forecasts generated by NWP models are described. Our proposed methods based on dynamical spatial models are presented as an automatic bias correction alternative for ensemble forecasting in longer training periods.

3.1 Static Calibration Models

The Model Output Statistics (MOS, [Glahn and Lowry, 1972](#)) defines a relation between an ensemble with m forecasts F_1, \dots, F_m , individually distinguishable, for an univariate quantity of interest Y through a multiple linear regression model which is given by

$$Y = \theta_0 + \theta_1 F_1 + \dots + \theta_m F_m + \varepsilon, \quad (1)$$

where the error term ε such that $E(\varepsilon) = 0$ and $Var(\varepsilon) = \sigma^2$.

An extension of MOS called Ensemble MOS (EMOS, [Gneiting et al., 2005](#)), also known as non-homogeneous regression, allows the response variance to depend on the dispersion of ensemble members. This improvement is termed as the spread-skill relationship. It is based on the premise that there is a positive relationship between ensemble spread and forecast absolute error. The EMOS method assumes that ε is such that

$$E(\varepsilon) = 0, \quad Var(\varepsilon) = \sigma_*^2 = \beta_0 + \beta_1 S^2, \quad (2)$$

where S^2 is the sampling variance of ensemble members and $\boldsymbol{\beta} = (\beta_0, \beta_1)'$ are non-negative coefficients. [Gneiting et al. \(2005\)](#) assumes Gaussianity and estimates model parameters by minimization of continuous ranked probability score (CRPS, [Matheson and Winkler, 1976](#)). Other applications of this method in the context of wind speed, strong winds and wind direction may be found in [Thorarinsdottir and Gneiting \(2010\)](#), [Thorarinsdottir and Johnson \(2012\)](#), and [Schuh et al. \(2012\)](#), respectively.

Spatial extension of MOS, the Geostatistical Output Perturbation (GOP, [Gel et al., 2004](#)) is the pioneer statistical postprocessing model which considers the correlation between the measurements of a meteorological variable at distinct locations. This technique produces calibrated forecasts for entire weather fields. Let $\{Y(\mathbf{s}), \mathbf{s} \in S \subset \mathbb{R}^2\}$ a random weather field and $\mathbf{Y} = (y(\mathbf{s}_1), \dots, y(\mathbf{s}_n))'$, an observed sample at n locations. Considering a set of m ensemble members for this locations, represented by $\mathbf{F}_1 = (F_1(\mathbf{s}_1), \dots, F_1(\mathbf{s}_n))', \dots, \mathbf{F}_m = (F_m(\mathbf{s}_1), \dots, F_m(\mathbf{s}_n))'$, and assuming $\boldsymbol{\varepsilon} = (\varepsilon(\mathbf{s}_1), \dots, \varepsilon(\mathbf{s}_n))'$, a vector of observations from a Gaussian Process $\{\varepsilon(\mathbf{s}), \mathbf{s} \in S\}$, such that

$$E(\boldsymbol{\varepsilon}) = \mathbf{0}_n, \quad \text{and} \quad Cov(\varepsilon(\mathbf{s}_i), \varepsilon(\mathbf{s}_j)) = \Sigma_{i,j} = \sigma^2 C(\mathbf{s}_i, \mathbf{s}_j), \quad i, j = 1, \dots, n, \quad (3)$$

where $\mathbf{0}_n$ is a zero n -vector and $C(\cdot, \cdot)$ is a valid spatial correlation function ([Cressie, 1993](#)) for any pair of locations in S . This method is a multivariate extension of the model described in (1) and therefore also does not allocate the ensemble information in its structure.

Finally, considering simultaneously the ensemble information and the spatial structure of meteorological variables, the Spatial EMOS (SEMOs, [Feldmann et al.,](#)

2015) is presented combining the EMOS and GOP models. It consists on GOP model formulation but assuming that

$$Cov(\varepsilon(\mathbf{s}_i), \varepsilon(\mathbf{s}_j)) = \Sigma_{i,j}^* = D_{i,i} C(s_i, s_j) D_{j,j}, \quad i, j = 1, \dots, n, \quad (4)$$

where $D = \text{diag}(\sqrt{\beta_0 + \beta_1 S_1^2}, \dots, \sqrt{\beta_0 + \beta_1 S_n^2})$ is a $n \times n$ diagonal matrix with S_i^2 representing the sample variance of ensemble members for location i . The models presented here, in their canonical form, are not appropriate for calibration of asymmetric variables (e.g. wind speed and rainfall).

3.2 Proposed dynamical calibration models

The postprocessing models proposed enhanced previous approaches in several ways, accounting for both, temporal dynamics and asymmetric distributions with mass at zero through a spatiotemporal modeling approach with censoring. These novel methods are presented as follows. In particular, the truncated Gaussian model which has been used in precipitation prediction (Bardossy and Plate, 1992; Sansó and Guenni, 1999) will be presented in the context of forecasts calibration from NWP models.

3.2.1 Spatiotemporal trans-Gaussian model

Let $\{Y_t(\mathbf{s}), \mathbf{s} \in S \subset \mathbb{R}^2, t = 1, \dots, T\}$ be a spatial random field in discrete time t . The observed response vector at n locations $\mathbf{Y}_t = (y_t(\mathbf{s}_1), \dots, y_t(\mathbf{s}_n))'$ is composed by censored variables, $y_t(\mathbf{s}_i) \geq c$, $i = 1, \dots, n$, $t = 1, \dots, T$. Assume that \mathbf{Y}_t follows a Truncated Gaussian distribution as follows:

$$Y_t(\mathbf{s}) = \begin{cases} BC^{-1}(X_t(\mathbf{s}), \lambda), & \text{if } BC^{-1}(X_t(\mathbf{s}), \lambda) > c, \\ c, & \text{if } BC^{-1}(X_t(\mathbf{s}), \lambda) \leq c, \end{cases} \quad (5)$$

where c is a known constant, λ is the unknown parameter of transformation, $X_t(\mathbf{s})$ is a Gaussian process and $BC(\cdot, \lambda)$ represents the family of Box-Cox transformations (Box and Cox, 1964) defined as

$$BC(y, \lambda) = \begin{cases} (y^\lambda - 1) / \lambda, & \text{if } \lambda \neq 0 \quad \text{and} \quad y > 0, \\ \log y, & \text{if } \lambda = 0 \quad \text{and} \quad y > 0. \end{cases}$$

Therefore, $X_t(\mathbf{s})$ is a latent Gaussian field which allows for asymmetry in the resulting process of interest $Y_t(\mathbf{s})$. That is, after transforming the possibly asymmetric process $Y_t(\mathbf{s})$, the resulting field will follow a Gaussian process.

Furthermore, censoring is admitted through a known constant c . In the context of wind speed calibration, c represents the minimum allowed value for observed wind speed (usually 0 m/s). However, depending on the application context, this

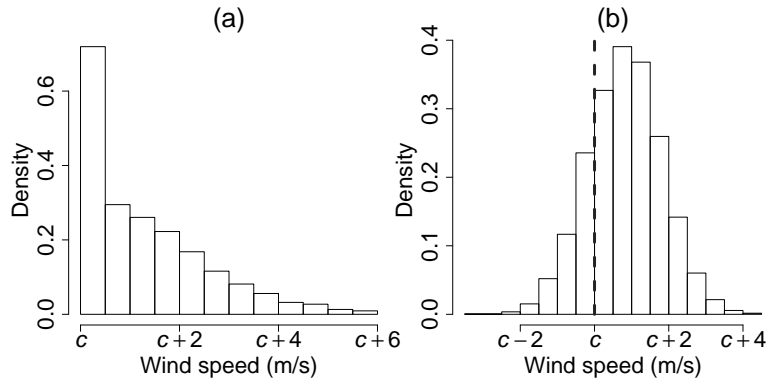


Figure 3: Histograms for (a) simulated wind speed and (b) transformed simulated wind speed by Box-Cox transformation as defined in (5). The dashed line represents the threshold value c .

value could be greater than zero. Figure 3 illustrates the practical effect of this modeling setup on simulated wind speed values at a single location. Note that values below c from transformed and truncated Gaussian latent process induce a mass at c in the process of interest $Y_t(\mathbf{s})$. The truncated Gaussian model has been useful in applied settings, such as precipitation modeling (Bardossy and Plate, 1992; Sansó and Guenni, 1999). The complete model with Box-Cox transformation and censoring is facilitated by the use of data augmentation techniques (Tanner and Wong, 1987). It also naturally allows for missing data.

In the usual setup for statistical calibration of numerical models time windows are defined to account for observed and predicted temporal variation, the called training period. Although larger training windows result in smaller uncertainty, it introduces distortions due to seasonal effects. In general, the seasonal patterns of meteorological variables are well defined (e.g. solar forcing – 24 hours and seasons – 3 months). Thus, the Kalman filter (Kalman, 1960) allows for both longer temporal training periods and inclusion of temporal dynamics in the bias parameters. As follows, we consider the Bayesian dynamical approach which considers the Kalman filter for forwarding filtering and the backward posterior smoothing for a fully Bayesian inference procedure as proposed by West and Harrison (1997). This approach allows for time-varying regression coefficients while accounting for spatial dependence in the region of interest, overcoming the over smoothing of numerical forecasts.

3.2.2 Dynamical Geostatistical Output Perturbation

The proposed model adds a temporal dynamic to the GOP formulation by allowing the coefficients to vary over time. The covariance modeling is stochastic

over time with Beta-Gamma evolution depending on discount factors. Assuming the structure stated in (5) for the transformation of the original process $Y_t(s)$, the dynamics are introduced by defining the observation and state equations as follows:

$$\mathbf{X}_t = \mathbf{F}'_t \boldsymbol{\theta}_t + \boldsymbol{\varepsilon}_t, \quad \boldsymbol{\varepsilon}_t \sim N(\mathbf{0}_n, \Sigma_t), \quad \Sigma_t = \varphi_t^{-1} H, \quad (6)$$

$$\boldsymbol{\theta}_t = \mathbf{G}_t \boldsymbol{\theta}_{t-1} + \boldsymbol{\omega}_t, \quad \boldsymbol{\omega}_t \sim T_{n_{t-1}}(\mathbf{0}_p, \mathbf{W}_t), \quad (7)$$

$$\varphi_t = \gamma_t \varphi_{t-1} / \delta^v, \quad \gamma_t \sim \text{Beta}(\kappa_t, \bar{\kappa}_t), \quad (8)$$

where $\boldsymbol{\varepsilon}_t = (\varepsilon_t(\mathbf{s}_1), \dots, \varepsilon_t(\mathbf{s}_n))'$ follows a zero mean multivariate normal distribution with covariance matrix $\Sigma_t = \varphi_t^{-1} H$ such that $\varphi_t = 1/\sigma_t^2$ is the precision and H , the correlation matrix with elements $H_{i,j} = C(\mathbf{s}_i, \mathbf{s}_j)$, $i, j = 1, \dots, n$. $C(\cdot, \cdot; \phi)$ is a valid correlation function depending on an unknown parameter ϕ . In particular, we assume $C(\mathbf{s}_i, \mathbf{s}_j; \phi) = \exp(-\phi \|\mathbf{s}_i - \mathbf{s}_j\|)$, the exponential correlation function, with $\phi > 0$ representing the exponential decay parameter and $\|\mathbf{s}_i - \mathbf{s}_j\|$, the Euclidean distance between locations \mathbf{s}_i and \mathbf{s}_j , $i, j = 1, \dots, n$. $\mathbf{X}_t = (x_t(\mathbf{s}_1), \dots, x_t(\mathbf{s}_n))'$, \mathbf{F}'_t is a matrix with dimension $n \times r$ ($r \geq m$) composed by covariates (e.g. predicted ensembles, latitude, longitude, and elevation) and $\boldsymbol{\theta}_t$ represents the state-space vector of variables with dimension r .

For the purely temporal components in (7) and (8), \mathbf{G}_t is an evolution matrix with dimension r , $\boldsymbol{\omega}_t$ are mutually independent follows a zero mean multivariate Student-t distribution with n_{t-1} degrees of freedom and unknown scale matrix \mathbf{W}_t which might be estimated using discounting factors. The degrees of freedom n_{t-1} and the shape parameters κ_t and $\bar{\kappa}_t$ are defined through a Beta-Gamma stochastic evolution (see [West and Harrison, 1997](#)). The parameter $\delta^v \in (0, 1]$ operates as a discount factor, then, the larger the discount, smaller the random shock in the observational covariance. When $\delta^v = 1$, the covariance is static over time, i.e., $\sigma_t^2 = \sigma^2, \forall t$. The initial information at time $t = 0$ assumes $\boldsymbol{\theta}_0 | \mathbf{D}_0 \sim T_{n_0}(\mathbf{m}_0, \mathbf{C}_0)$ and $\varphi_0 | \mathbf{D}_0 \sim G(n_0/2, d_0/2)$.

3.2.3 Spatiotemporal Ensemble Model Output Statistics

Analogously to the model in (3.2.2), this proposed model combines the Spatial EMOS with DLMs. Also assuming the structure stated in (5), the spatiotemporal Gaussian model for $X_t(s)$ is given by:

$$\mathbf{X}_t = \mathbf{F}'_t \boldsymbol{\theta}_t + \boldsymbol{\varepsilon}_t, \quad \boldsymbol{\varepsilon}_t \sim N(\mathbf{0}_n, \Sigma_t^*), \quad (9)$$

$$\boldsymbol{\theta}_t = \mathbf{G}_t \boldsymbol{\theta}_{t-1} + \boldsymbol{\omega}_t, \quad \boldsymbol{\omega}_t \sim N(\mathbf{0}_p, \mathbf{W}_t), \quad (10)$$

where $\boldsymbol{\varepsilon}_t = (\varepsilon_t(\mathbf{s}_1), \dots, \varepsilon_t(\mathbf{s}_n))'$ follows a zero mean multivariate normal distribution with covariance matrix Σ_t^* with elements $\Sigma_{t,i,j}^* = D_{t,i} H_{i,j} D_{t,j}$, $i, j =$

1, ..., n , with also $H_{i,j} = \exp(-\phi\|\mathbf{s}_i - \mathbf{s}_j\|)$ and $D_t = \text{diag}\left(\sqrt{\beta_0 + \beta_1 S_{1,t}^2}, \dots, \sqrt{\beta_0 + \beta_1 S_{n,t}^2}\right)$, a n -dimensional diagonal matrix, such that $S_{i,t}^2$ is the sample variance of the ensemble forecast for the location i at time t . Different from the model in (3.2.2), ω_t is normally distributed with unknown covariance matrix \mathbf{W}_t which might also be estimated using discounting factors. The initial information at time $t = 0$ assumes $\boldsymbol{\theta}_0 | \mathbf{D}_0 \sim N(\mathbf{m}_0, \mathbf{C}_0)$.

3.3 Inferential procedure

Let $\mathbf{y} = (\mathbf{y}_1, \dots, \mathbf{y}_T)$ be the collection of T observed time series at n spatial locations over $S \subset \mathbb{R}^2$ and, $\Theta = (\boldsymbol{\theta}_{0:T}, \sigma_{0:T}^2, \phi, \lambda)'$ and $\Theta^* = (\boldsymbol{\theta}_{0:T}, \boldsymbol{\beta}, \phi, \lambda)'$ be the parameter vector in (3.2.2) and (3.2.3), respectively, such that $\boldsymbol{\theta}_{0:T} = (\boldsymbol{\theta}_0, \dots, \boldsymbol{\theta}_T)$ and $\sigma_{0:T}^2 = (\sigma_0^2, \dots, \sigma_T^2)$.

The inference procedure is performed under the Bayesian paradigm and model specification is complete after assigning a prior distribution for the parameter vector Θ and Θ^* . An advantage of following the Bayesian paradigm is that the inferential procedure is performed under a single framework and uncertainty about parameters estimation is naturally accounted for. Moreover, uncertainty about spatial interpolations and temporal predictions is naturally described through the credible intervals (CI) of the respective posterior predictive distributions. Assuming that the components of Θ and Θ^* are independent *a priori*, we get by Bayes' theorem the following posterior distribution for Θ :

$$\begin{aligned} p(\Theta | \mathbf{y}) \propto & \prod_{t=1}^T |\Sigma_t|^{-1/2} \exp \left\{ -\frac{1}{2} \sum_{t=1}^T (\mathbf{X}_t - \mathbf{F}'_t \boldsymbol{\theta}_t)' \Sigma_t^{-1} (\mathbf{X}_t - \mathbf{F}'_t \boldsymbol{\theta}_t) \right\} \\ & \times \exp \left\{ -\frac{1}{2} \sum_{t=1}^T (\boldsymbol{\theta}_t - \mathbf{G}_t \boldsymbol{\theta}_{t-1})' \mathbf{W}_t^{-1} (\boldsymbol{\theta}_t - \mathbf{G}_t \boldsymbol{\theta}_{t-1}) \right\} \\ & \times \prod_{\{i,t: y_{it} > c\}} y_{it}^{\lambda-1} \times p(\Theta). \end{aligned} \quad (11)$$

The posterior distribution for Θ^* is obtained analogously. The prior distributions assigned to, respectively, Θ and Θ^* are described in Section 4.1.

The kernel of this distribution does not result in a known closed-form expression. Markov chain Monte Carlo (MCMC) methods are considered to obtain samples from the posterior distribution of interest. In particular, Gibbs sampler algorithm is used when there are missing or censored observations, i.e., respectively, $Y_t(s)$ is missing or $Y_t(s) \leq c$; the forward filtering backward sampling algorithm (FFBS, Frühwirth-Schnatter, 1994; Carter and Kohn, 1994) for $\boldsymbol{\theta}_{0:T}$ and $\sigma_{0:T}^2$; and the robust adaptive Metropolis algorithm (RAM, Vihola, 2012) for the remaining parameters.

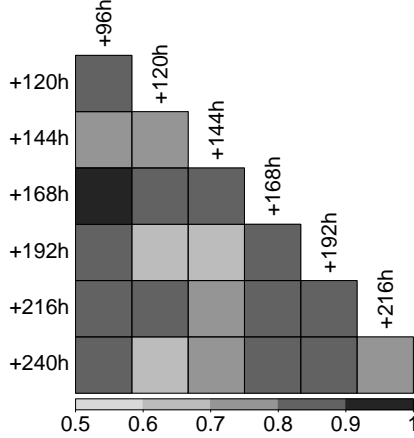


Figure 4: Correlation matrix of the ensemble forecast members for wind speed at 10 meters on 21 June 2016, 1200 UTC. The labels represent the horizon of forecast for each member.

4 Application to wind speed forecasts in the state of Minas Gerais

Following the motivation presented in sections 1 and 2, the proposed postprocessing extensions are used in this section for calibrating hourly wind speed forecasts (24 hours ahead) for the state of Minas Gerais generated by the Eta regional climate model. In particular, we consider a subset of 59 weather stations and a random selection of 20 days per season from the temporal range of the available dataset. Thus, the overall and per season results aggregate predictions for 20 days (480 hours) and 80 days (1920 hours), respectively. The results are compared with those obtained under current postprocessing approaches. In this application, we assess the overall performance of the postprocessing approaches in terms of minimizing systematic errors of wind speed forecasts throughout the study region.

4.1 Model settings

For each fitted model, the same mean structure is defined depending on the mean of the ensemble of wind speed forecasts and a set of auxiliary variables defined at each location: roughness length (see calculation details in Appendix A), latitude, longitude, and elevation. Thus, matrix \mathbf{F}'_t in (6) has row components

$$(1, \bar{f}(s_i), \text{roughness}(s_i), \text{elevation}(s_i), \text{latitude}(s_i), \text{longitude}(s_i), 1, 0)'.$$

The ensemble mean \bar{f} was used to avoid eventual unavailability of any ensemble member and multicollinearity problems. This procedure does not entail a great loss of information, since there is a high linear correlation between the members, as shown in Figure 4, implying a reasonable stability of the numerical forecasts from Eta model. According to [Grimit and Mass \(2007\)](#), the ensemble mean may capture a possible point anomaly (e.g. cold front) and thus its use is also indicated by theoretical aspects. The seasonal pattern of solar forcing was represented by a Fourier harmonic through evolution matrix \mathbf{G}_t which is nested on dynamic linear models. In particular, this matrix is given by $\mathbf{G}_t = \text{diag}(\mathbf{G}_1, \mathbf{G}_2)$, with \mathbf{G}_1 is an identity matrix of order 6 and

$$\mathbf{G}_2 = \begin{pmatrix} \cos(2\pi/24) & \sin(2\pi/24) \\ -\sin(2\pi/24) & \cos(2\pi/24) \end{pmatrix}.$$

To simplify the inference procedure established in Section 3.2, the covariance matrix of the evolution equation \mathbf{W}_t in (7) and (10) is estimated using discounting factors ([West and Harrison, 1997](#)). We set the discount factors δ_T for trend referring to the intercept, the numerical prediction and the geographic location components, and δ_S for seasonality component. The discount factor δ_v is exclusive for the DGOP model and, for the GOP model, it works as an artificial instrument to insert random shocks in the observational covariance along time, as shown in (8). Moreover, we assigned reasonably vague priors to model parameters. Specifically, for exclusive parameters of DGOP: $\boldsymbol{\theta}_0 \sim T_1(\mathbf{0}, \mathbf{I}_8)$ where \mathbf{I}_8 is an identity matrix of order 8 and $\varphi \sim G(1, \frac{1}{10})$; for exclusive parameters of STE-MOS: $\boldsymbol{\theta}_0 \sim N(\mathbf{0}_8, \mathbf{I}_8)$ and $\boldsymbol{\beta} \sim NT_{(0,\infty)}(\mathbf{0}_2, 10\mathbf{I}_2)$; and for common parameters: $\lambda \sim N(1, 10)$ and $\phi \sim G\left(2, \frac{\max(d)}{6}\right)$ based on the assumption that the practical range (when the spatial correlation is equal to 0.05) is reached at half of the maximum distance ($\max(d)/2$) between weather stations locations.

To evaluate the improvements in the calibration of wind speed forecasts for the state of Minas Gerais, six models were fitted to the dataset described in Section 2. The models were obtained from distinct settings of the proposed models, which are described in Table 1. All configurations considered the left censoring with Box-cox transformation as described in (5). Establishing certain parameters of the proposed models on specific values, we obtain simpler models as particular cases. For instance, if the discount factors are set to 1, the corresponding dynamic parameters become static over time. Setting the transformation parameter λ equals to 1, the Box-Cox transformation results in keeping the response in its original scale. Finally, when a large value is assigned to the decay parameter of the exponential correlation function ϕ , the correlation matrix H in (6) and (9) tends to an identity matrix resulting in spatial independence between observed locations. We used a moving window training dataset of 10 days (240 hours) as a

Table 1: Summary of features and discount factor setup for fitted models on the calibration process of wind speed forecast at 10 meters from Eta model.

Model	Features		Discount factors		
	Dynamic parameters	Spatial component	δ_t	δ_s	δ_v
MOS	No	No	1	1	-
GOP	No	Yes	1	1	1
SEMODS	No	Yes	1	1	-
DMOS	Yes	No	.99	.95	-
DGOP	Yes	Yes	.99	.95	.99
STEMOS	Yes	Yes	.99	.95	-

training period.

4.2 Computational details

The MCMC algorithm was implemented in the R programming language, version 3.4.1 ([R Core Team, 2017](#)). To speed up this simulation process, some particular functions were implemented in C++ language using the library **Armadillo** ([Sanderson and Curtin, 2016](#)) through the package **Rcpp** ([Eddelbuettel et al., 2011](#)). The analyses were carried out using a laptop computer with a 2.70 GHz Intel Core i7-7500 processor, 32 GB RAM, running under a Microsoft Windows 7 Professional operating system.

For each fitted model over time, convergence tests were made for check agreement and convergence of two parallel chains starting from different values. The convergence diagnostic was given through the dependence factor ([Raftery and Lewis, 1995](#)) and the \hat{R} statistics ([Gelman et al., 1992](#)). With chains convergence ensured by these tests, we ran operationally a single chain with 12,500 iterations, discarding the first 500 and sampling at every 5th step.

4.3 Results

Model comparison is performed through the out-of-sample predictive performance using the square root of the mean square error (RMSE), the mean absolute error (MAE), the index of agreement (d , [Willmott, 1981](#)), and the interval score (IS, [Gneiting and Raftery, 2007](#)). Each of these criteria are described in more detail in Appendix B. The computational efficiency also used as a secondary model comparison criteria. Table 2 reports the average of the MAE, RMSE, d , IS, and computational time (in minutes) for 24-h wind speed forecasts at 10 meters ob-

Table 2: Average MAE, RMSE, d , IS, and computational time (in minutes) of 24-h deterministic forecasts for wind speed at 10 meters.

Forecast	MAE	RMSE	d	IS	Time (min)
Ensemble mean	1.66	1.95	0.48	-	-
<i>Static models</i>					
MOS	1.07	1.32	0.44	21.90	60.22
GOP	1.07	1.33	0.42	78.74	74.13
SEMODS	1.08	1.33	0.42	46.23	81.34
<i>Dynamic models</i>					
DMOS	0.94	1.17	0.57	4.10	58.76
DGOP	0.94	1.19	0.58	4.38	86.29
STEMOS	0.94	1.19	0.58	4.49	89.73

tained under Eta model and the six fitted models. All the fitted models present better results than the ensemble mean for all the criteria considered. In particular, models considering temporal dynamics performed better than the others for all criteria. Considering MAE criteria, they were better than ensemble mean and the best static model (MOS), respectively, in 43% and in 13%. Similar results were obtained in terms of the RMSE. With respect to the index of agreement d , while the ensemble mean performed better than the static models, the dynamic models outperformed the ensemble mean by 20% and the static models by 32%. Then, considering the prediction intervals of probabilistic forecasts, the static models obtained the highest values of IS. Moreover, IS criterion allowed to point out clearer differences between the dynamic models than the other criteria considered. In particular, DMOS presented the smallest value for the IS criterion. Additionally, the boxplots of this average model comparison criteria of 24-h deterministic forecasts for wind speed at 10 meters over the seasons are provided as additional figures in Appendix C. It shows that the forecast evaluation criteria considered, as well as wind speed, have different patterns across seasons. About computational time, the DGOP-based models were more efficient on average, taking about 2.4% to 8.9% less time than STEMOS-based models fitting. Its better performance is related to the sequential estimation of dynamic parameters.

Among the model comparison criteria considered, the RMSE has a particular feature that can be used to discriminate different error sources in the context of calibration of wind speed forecasts. In general, error sources are related to either local conditions or general properties of the NWP models. According to [Lange \(2005\)](#), this criterion can be decomposed into two additive parts: the amplitude and the phase errors. Figure 5 shows illustrative panels for each of these additive components recorded at Viçosa weather station. In some cases these components

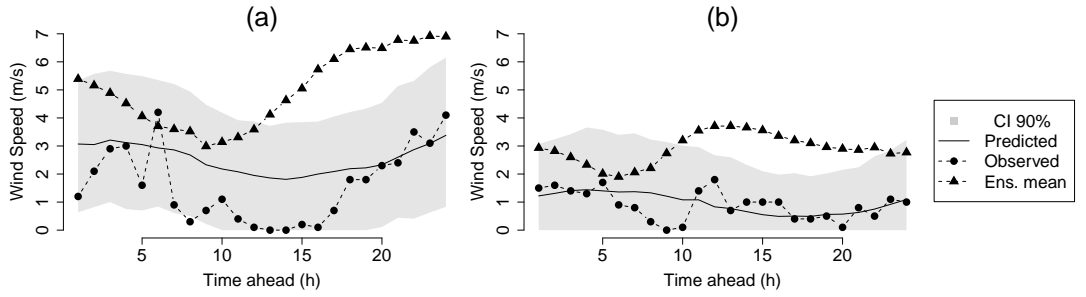


Figure 5: DGOP 24-h probabilistic forecast window for wind speed at 10 meters for Viçosa weather station from (a) 08 November 2016, 1300 UTC to 09 November 2016, 1200 UTC and (b) 12 April 2017, 1300 UTC to 13 April 2017, 1200 UTC. The solid circles represent the numerical prediction. The solid triangles represent the actual values, the solid line represents the bias-corrected deterministic forecasts, and the shaded area represents the 90% prediction interval.

maybe not explicitly well-defined generating a clear visualization. Generally, both occur but with different intensities. The amplitude errors are related to forecasts with correct temporal evolution but with a systematic difference from the actual measure. An observation of this error type is shown in Figure 5(a). Note the similarity of the trajectory between both predictions and actual values, except for the level. On the other hand, the phase errors are related to forecasts with correct amplitude but with a mismatch on the temporal evolution of the actual measure. Figure 5(b) shows a case for which the numerical forecast does not respect the duration of the intraday seasonal cycle. This can be considered a phase error. Specific corrections are indicated for each component of the error. Statistical postprocessing methods apply linear corrections and can minimize amplitude errors. However, this process is ineffective for phase errors, which are associated with cross-correlation between the forecast and actual time series. Thus, this error type is invariant under linear transformations. Panels of Figure 6 display the decomposition components of RMSE for deterministic forecasts from probabilistic models over the seasons. Figure 6(a) shows the portion of RMSE associated to phase errors. For all seasons, the forecast errors of dynamic models present lower values for this component than the static models. Among the dynamic models, the full-featured models associate its RMSE values slightly less to phase errors than the simplest model DMOS. By this way, as the decomposition elements of RMSE are complementary, the models DGOP and STEMOS associate greater parts of RMSE value to the amplitude errors when compared to other models, as shown in Figure 6(b).

A larger portion of RMSE associated with amplitude errors still allows substantial improvements through linear corrections. Thereby, the dynamic models have

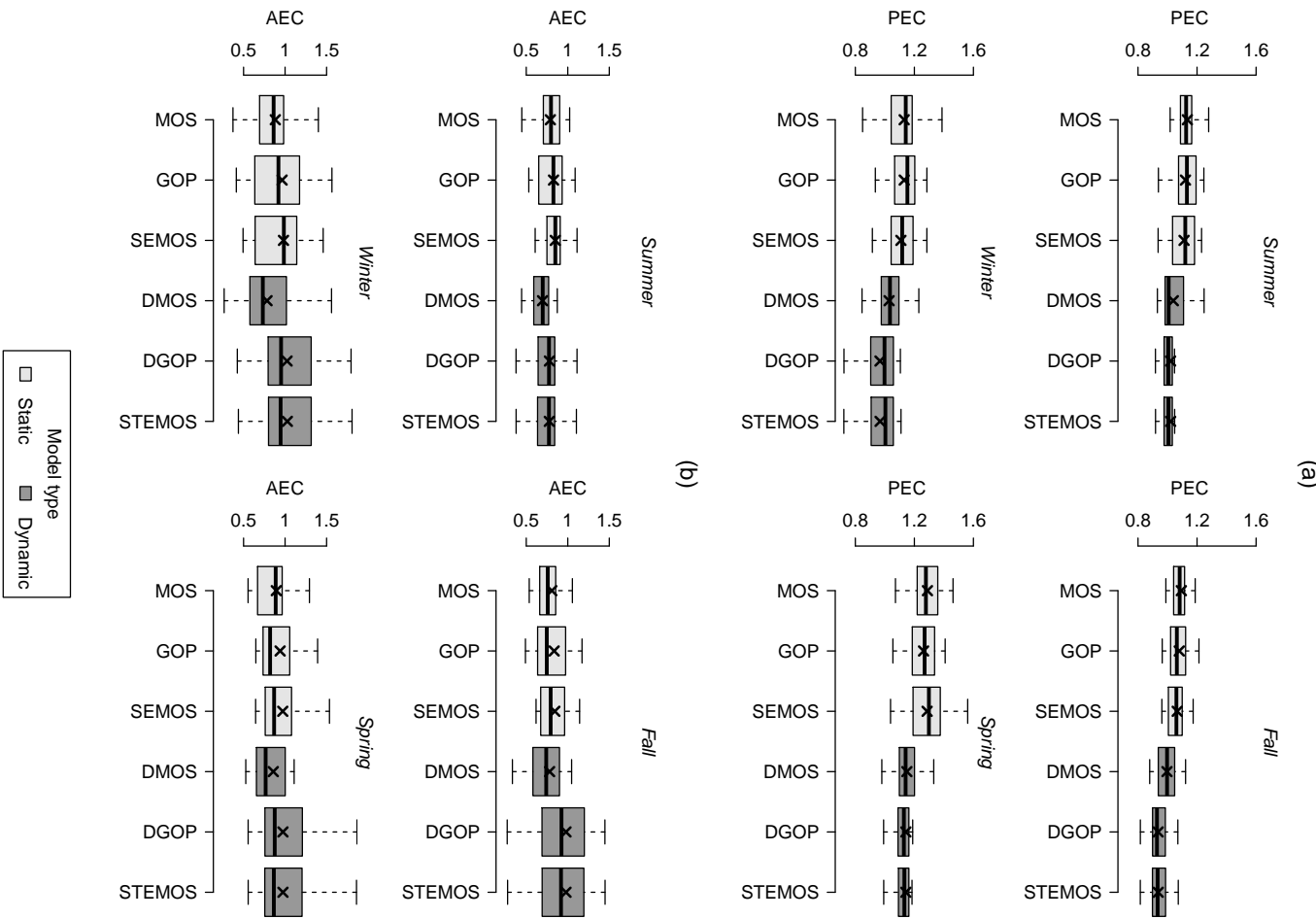


Figure 6: Boxplots of average decomposition of RMSE: (a) phase errors component (PEC) and (b) amplitude errors component (AEC) of 24-h deterministic forecasts for wind speed at 10 meters over the seasons. The horizontal dense line and the \times symbol in each boxplot represent respectively, the median and the mean values.

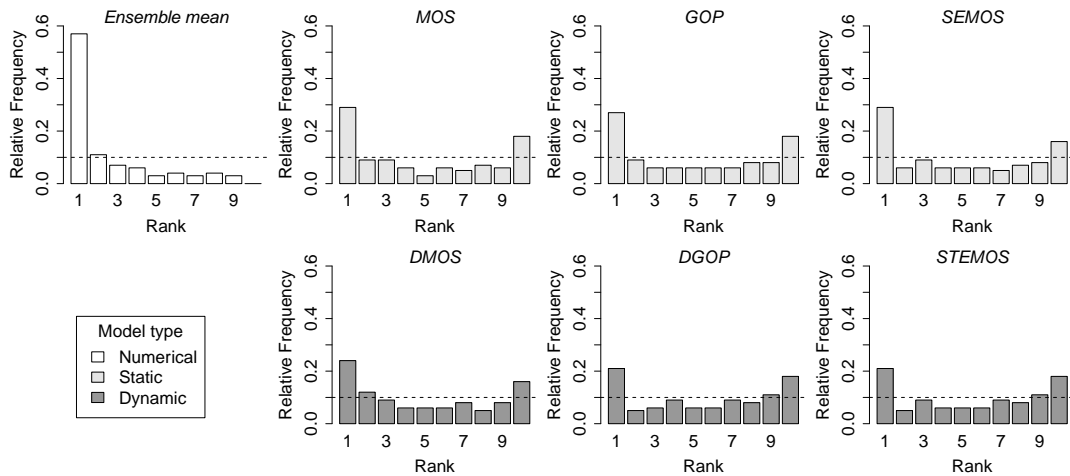


Figure 7: Verification rank histograms of forecasts for wind speed at 10 meters over Minas Gerais.

greater potential for better calibrated probabilistic predictions among all fitted models. These benefits can be obtained by including more covariate information about the local pattern of the weather phenomenon or more detailed geographical features of relief (e.g. climatology, vegetation type and presence of water bodies).

An overall calibration assessment of forecasts was made through the verification rank histogram (Anderson, 1996) which evaluates the forecasts reliability. An ideal calibration is obtained when its bins are uniformly distributed. Figure 7 shows the verification rank histograms for forecasts from all fitted models considering the aggregate result for all period and weather stations over Minas Gerais. The skewed aspect of the histogram for forecasts obtained by the ensemble members means implies that the measurements at weather stations are lower than its predictions, i.e., the ensemble mean commonly overestimates the actual values. All tested calibration models significantly improve numerical forecasts. Specifically, the forecasts from statistical postprocessing models present similar histograms. These histograms have aspect closer to a uniform distribution than the histogram for uncalibrated forecasts. This result indicates greater reliability. Indeed, the calibration process removes the systematic error resulting in more accurate forecasts as shown in Table 2. The forecasts from dynamic models have slightly less under dispersed distribution. Among these, the DGOP and the STEMOS present best calibration overall. Nevertheless, the observed U-shaped aspect can represent a lack of variability. The irregularities of boundary bins (bins 1 and 10) suggest that the calibrated forecasts are not ideal at outermost values. According to wind speed measurements at all weather stations over Minas Gerais, we interpret the outermost values as 0.2 and 3.8, respectively 0.1 and 0.9-quantiles.

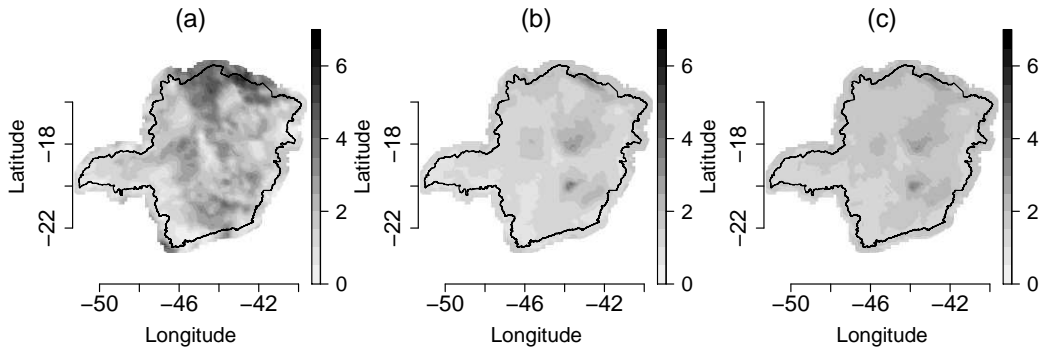


Figure 8: 24-h weather field forecast of wind speed at 10 meters over the State of Minas Gerais on 21 July 2016, 1200 UTC: (a) Numerical prediction, (b) DGOP deterministic forecast, and (c) DGOP margin of error defined as half the width of the 90% prediction interval.

The models with spatial component (see Table 1) allow straightforward spatial interpolation through kriging (Cressie, 1993) assuming that the latent process $X_t(\mathbf{s})$ in (5) is a realization of the Gaussian Random Fields. Thereby, potential improvements in site forecasts may be obtained from the proposed statistical post-processing processes over the entire weather field. Figure 8 shows the 24-h weather field forecast of wind speed at 10 m height over the State of Minas Gerais initialized on 21 July 2016, 1200 UTC. Figure 8(a) shows the numerical prediction for the entire weather field obtained using the bilinearly interpolated mean of ensemble forecasts. Figure 8(b) shows the deterministic DGOP weather field forecast defined as the median of the predictive distribution. Note that the calibrated forecasts were smoothly spatially distributed in contrast to the numerical prediction. As shown in Figure 7, the ensemble members from the Eta model, specifically the ensemble mean, generally overestimate the actual wind speed at 10 meters. Thus, bias-corrected smooth distribution over the weather field has greater reliability. Lastly, Figure 8(c) shows the margin of error of the 90% prediction interval defined as half the width of the credible interval. This plot is useful to indicate regions where there is more uncertainty in predictions. Three regions in the map, closer to the center, are spotted as having larger variability.

Regarding model parameters fitting and interpretation, Figure 9 shows the posterior distribution behavior of selected parameters from DGOP. Figure 9(a) shows boxplots of the average median for the estimated posterior distribution of the Box-Cox transformation parameter λ over the seasons. The Gaussian model, corresponding to $\lambda = 1$, is not selected for this application in any season. The square root transformation is supported for summer, fall, and winter. For the spring which records the highest wind speeds, it is suggested a transformation of $\lambda = 0.6$ approximately. These results indicate that the data transformation

should not be restricted to a single and static transformation. Figure 9(b) shows boxplots of average practical range for the estimated posterior distribution of the decay parameter ϕ over the seasons. Again, the practical range represents the distance where the spatial correlation between the weather stations decays until to be virtually null. For example, this distance is on average estimated at 35 km approximately in winter. In practice, the weather stations within an approximately 2 grid cell radius are correlated to each other since the Eta model grid has a resolution of 15 km (see Figure 1). Except for winter, the variance of the average practical range is large. The estimate for spring varies between 27.3 to 82.1 km with a standard deviation of 16 km. Similar amplitude and deviation were estimated for summer. These values are evidence that the decay parameter can vary hourly and spatially. The current proposal does not accommodate non-stationarity in the spatial parameters. For both static parameters exhibited, the values decays during fall and winter. Conversely, they increase during summer and spring. This may imply the existence of an annual seasonal cycle for these parameters. Finally, 9(c) shows the behavior of the average path for the estimated posterior distribution of the intercept parameter θ_0 from DGOP model over spring and winter during the training period. Again, this moving window has a length of 240 hours (10 days). In the postprocessing context, the intercept parameter is applied as an additive bias correction. The cyclic movements are uniform and appear to evolve around a constant average over the winter. In contrast, they present irregular temporal evolution during spring. Note that for both seasons displayed, θ_0 assumes negative values. This implies that there is a positive additive bias, i.e., the forecasts from the Eta model usually overestimate the wind speed at 10 meters. This fact endorses the arguments about Figure 7.

5 Discussion

This work presents two new statistical calibration models for forecasts obtained from regional climate models for entire weather fields. The proposed models generalize the well-established spatial postprocessing techniques GOP and SEMOS by combining them with Bayesian dynamic models. Thus, the proposed methods take into account the spatial and temporal correlations, allowing the spatiotemporal calibration of forecasts obtained from NWP models. As discussed in Section 1, the homogenization of topographic relief made by the NWP models results in outputs with potential spatially correlated errors. Thus, the calibration made through geostatistical models preserves the inherent spatial correlation structure of the weather field. Additionally, the intrinsic seasonal patterns of meteorological phenomena, discussed in Section 3, motivate the use of postprocessing techniques that include temporal correlation on the calibration process as the Bayesian dy-

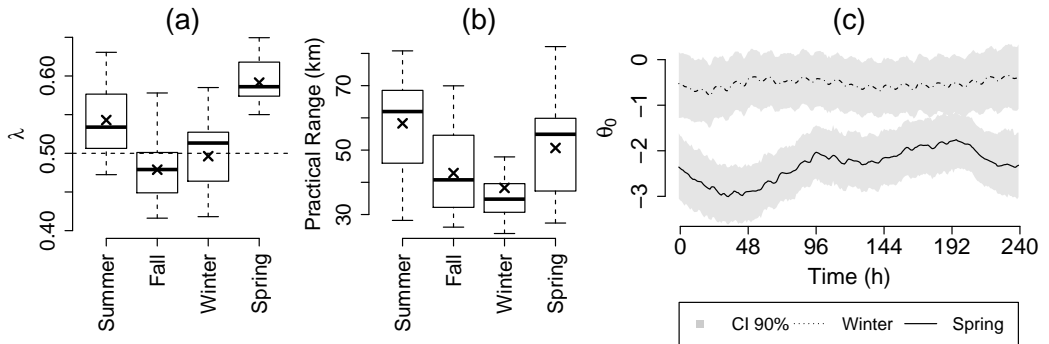


Figure 9: Boxplots of (a) average median for the estimated posterior distribution of the Box-Cox transformation parameter λ over the seasons and (b) average practical range for the estimated posterior distribution of the decay parameter ϕ over the seasons. (c) Average path for the estimated posterior distribution of the intercept parameter θ_0 from DGOP model over spring and winter. The dashed line in (a) represents the square root transformation. The horizontal dense line and the \times symbol in each boxplot represent respectively, the median and the mean values.

namic models do. In contrast with the well-established calibration methods that result a single forecast for a fixed horizon, the proposed methods allow a single sequential calibration over time, more suitable for hourly data, producing a bias-corrected forecast window output. Moreover, the dynamic structure avoids the issue of optimizing empirically the length of training period due to the intrinsic ability to weight past observations over time (see [West and Harrison, 1997](#)). As [Raftery et al. \(2005\)](#) suggest, the proposed methods provide an automatic way of choosing the length of the training period. This is balanced such that, from a minimum length threshold, parameter estimation is not affected, thus avoiding distortions on the calibration process. Also, other advantages of our methods are the natural manipulation of missing data and the versatility of models. Through the data augmentation technique, the missing data is interpreted as latent data and parameter estimation is performed by a fully Bayesian approach, without large computational cost.

In particular, we investigate the calibration process of wind forecasts at 10 meters, which are well known to be locally predicted with systematic errors. As discussed in Section 2, these errors are associated with the complex landscapes of Minas Gerais and its strong influence on wind speed behavior at low heights. The study region can be considered a low wind speed area. Figure 2 shows a common pattern recorded at the 68 weather stations: a large amount of zero observations, rare wind speeds above 6 m/s, skewed distribution and different wind speed behavior from other seasons during spring. These characteristics are also commonly observed in many precipitation modeling and forecasting applications. Following

the application made by [Sansó and Guenni \(1999\)](#), the proposals introduce data transformation within the dynamical model, resulting in a flexible sampling distribution for the errors, which could be potentially asymmetric. Hence, our approach leads to narrower predictions when compared to the simpler models without temporal dependence. In this application, the space-time models result in an overall slightly better calibration performance, as shown in Table 2 of Section 4.3. By the decomposition of RMSE, explored also in Figure 6, it is observed that the proposed models associate more parts of its RMSE with amplitude errors which can still be corrected through linear transformations. This association implies that potential improvements can still be made by including additional information using auxiliary variables. Among the probabilistic models, DGOP and STEMOS produced more reliable forecasts, as shown in Figure 7. The persistence of U-shaped aspect of verification rank histograms indicates a lack of variability. However, the specific irregularities in boundary bins can also be an indicator of conditional biases. [Hamill \(2001\)](#) suggests a local exploratory analysis of model fit and forecast variability. Given the massive variability of Minas Gerais relief, the simplistic geostatistical models (see Table 1) may also underestimate local characteristics. The exponential correlation function was used due to its good functionality and applicability in the calibration context, as seen in [Gel et al. \(2004\)](#) and [Feldmann et al. \(2015\)](#).

The inference procedure was made through a fully Bayesian approach. The required prior distributions assigned for model specification was weakly informative. This approach has attractive differentials such as naturally taking into account the uncertainty about parameter estimation, but it is still quite expensive computationally as shown in Table 2. At the time, it is indicated only for medium-term and long-term forecasts.

Finally, useful structural improvements can be made, for example, by weighting each available ensemble member as proposed by [Scheuerer et al. \(2015\)](#). We work with a particular case in which the same weight is given for each member, i.e., the ensemble (arithmetic) mean. [Feldmann et al. \(2015\)](#) also proposed the inclusion of local climatological information through auxiliary variables. The proposed models might also be applied to space-time calibration of other asymmetric censored meteorological variables forecasts (e.g. precipitation) from grid-based NWP models, which its regime influences seasonal patterns. Additional research on this subject is currently underway.

Acknowledgements

The authors would like to thank Dr. Chou Sin Chan (CPTEC/INPE) for providing the Eta model outputs used in this study and for her advice during

the research. The first author also thank the financial support from the partnership between the Fundação de Amparo à Pesquisa do Estado de Minas Gerais (FAPEMIG) and the Companhia Energética de Minas Gerais S.A. (CEMIG) under Project APQ-03813-12.

A Calculation of the roughness length

According to [Hansen \(1993\)](#), the vegetation present on a surface influences the aerodynamic roughness characteristics encountered by the mean wind flow over that surface, affecting both the mean wind speed and direction predicted by models, and various other atmospheric parameters. Therefore, the surface roughness length, z_0 , defined as the height at which the wind speed equals zero, has an important role in the modelling of atmospheric processes.

The aerodynamic roughness length parameter, z_0 , used as a covariate in the application, was estimated for each calibration site from key atmospheric variables, following some principles of the Monin-Obukhov Similarity Theory ([Monin and Obukhov, 1954](#)). Particularly, assuming a logarithmic wind profile, the averaged wind speed \bar{u}_i at height z_i (10 meters), given by

$$\bar{u}_i = \frac{u_*}{k} \left[\ln \left(\frac{z_i}{z_0} \right) - \Psi(\zeta_i) \right] \quad (12)$$

was used to derive the roughness length z_0 as

$$z_0 = z_i \exp \left(\frac{-\bar{u}_i k}{u_*} - \Psi(\zeta_i) \right), \quad (13)$$

where k is the von Karman constant, u_* is the friction velocity, $\Psi(\zeta_i)$ is the stability correction function of the wind profile and $\zeta_i = \frac{z_i}{L}$ is the non-dimensional stability parameter given by the height above ground, z_i , normalized by the Obukhov length, L .

Measurements of air temperature, air pressure, sensible heat flux, momentum flux and wind stress can be used to derive u_* , L and $\Psi(\zeta_i)$ parameters. In this application hourly air temperature and air pressure data were obtained from the available meteorological stations, while hourly reanalysis data coming from the CFSV2 model ([Saha et al., 2014](#)) were used as the source of heat and momentum fluxes, after interpolation from the CFSV2 regular grid to the calibration sites.

Hourly values of the roughness length, z_0 , were firstly obtained from (13) for the two years of available data. Then, median values of z_0 by month and by hour within each month (288 values in total for each calibration site) were calculated, considering only those z_0 values that were estimated during neutral conditions of atmospheric stability (such condition is achieved when $|L| > 500$).

B Model comparison criteria

In this section, we briefly describe the model comparison criteria used to compare the prediction of fitted models in Section 4. The first three criteria (RMSE, MAE and Index of agreement) are appropriate to compare numerical predictions from the Eta model, which provides only deterministic estimates, with the proposed postprocessing models. The probabilistic forecasts are evaluated through IS, which takes into account the amplitude and coverage of the prediction intervals in a parsimonious way.

B.1 Mean absolute error and square root of the mean square error

Standard measures of goodness of fit were also entertained in this study for comparison purposes. The square root of the mean square error (RMSE) and the mean absolute errors (MAE) are given by:

$$\text{RMSE} = \frac{1}{nT} \sum_{i=1}^n \sum_{t=1}^T (y_t(s_i) - \hat{y}_t(s_i))^2 \quad \text{and} \quad \text{MAE} = \frac{1}{nT} \sum_{i=1}^n \sum_{t=1}^T |y_t(s_i) - \hat{y}_t(s_i)|,$$

where $\hat{y}_t(s_i)$ is obtained through a Monte Carlo estimate of the posterior mean of the predictive distribution, that is, $E[y_t(s_i) | \mathbf{y}]$, across N draws. Smaller values of RMSE and MAE indicate the best model among the fitted ones.

B.2 Index of agreement

Willmott (1981) introduced a standard measure for assessing the quality of forecasts. The index of agreement (d) ranges between 0 (absence of agreement) and 1 (perfect agreement) and is given by:

$$d = 1 - \frac{\sum_{i=1}^n \sum_{t=1}^T (y_t(s_i) - \hat{y}_t(s_i))^2}{\sum_{i=1}^n \sum_{t=1}^T (|\hat{y}_t(s_i) - \bar{y}| + |y_t(s_i) - \bar{y}|)^2},$$

where $\bar{y} = \frac{1}{n} \sum_{i=1}^n \sum_{t=1}^T y_t(s_i)$.

B.3 Interval score

The interval score (IS, Gneiting and Raftery, 2007) is a scoring rule for interval predictions considering the symmetric prediction interval with level $(1 - \alpha) \times 100\%$. The score is rewarded by accurate intervals and penalized when there is no coverage

of the forecast. If actual values are contained in the prediction interval, this measure is reduced to the range amplitude. The average IS is given by:

$$\begin{aligned} \text{IS} = & \frac{1}{nT} \sum_{i=1}^n \sum_{t=1}^T (\hat{u}_t(s_i) - \hat{l}_t(s_i)) \\ & + \frac{2}{\alpha} (\hat{l}_t(s_i) - y_t(s_i)) \mathbb{1} \{ y_t(s_i) < \hat{l}_t(s_i) \} \\ & + \frac{2}{\alpha} (y_t(s_i) - \hat{u}_t(s_i)) \mathbb{1} \{ y_t(s_i) > \hat{u}_t(s_i) \} \end{aligned}$$

where $\hat{l}_t(s_i)$ and $\hat{u}_t(s_i)$ are, respectively, the lower bound obtained by the $\frac{\alpha}{2}$ quantile, and the upper bound, obtained by the $1 - \frac{\alpha}{2}$ quantile of the based on the predictive distribution. The indicator function is represented by $\mathbb{1}$.

Smaller IS values indicate probabilistic forecasts more efficient.

C Supplementary results

The forecasts from numerical and static probabilistic models were omitted from the Figure 13 for clarity of exposition.

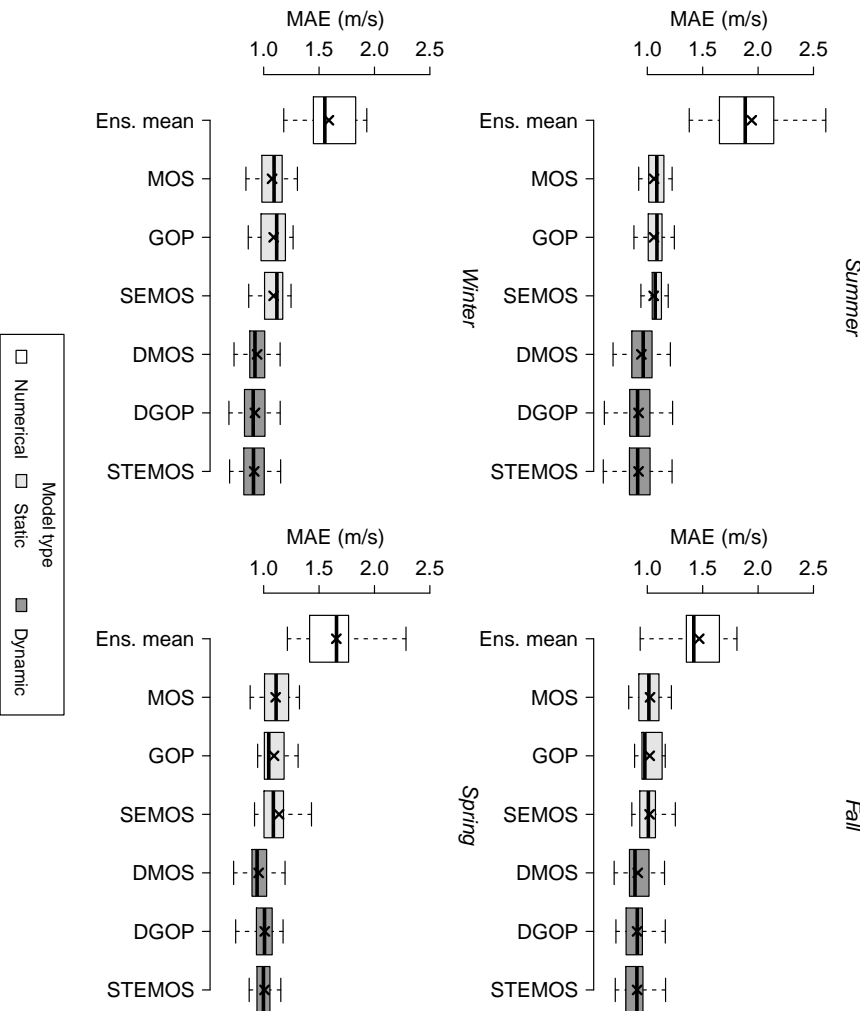


Figure 10: Boxplots of average MAE of 24-h deterministic forecasts for wind speed at 10 meters over the seasons. The horizontal dense line and the \times symbol in each boxplot represent respectively, the median and the mean values.

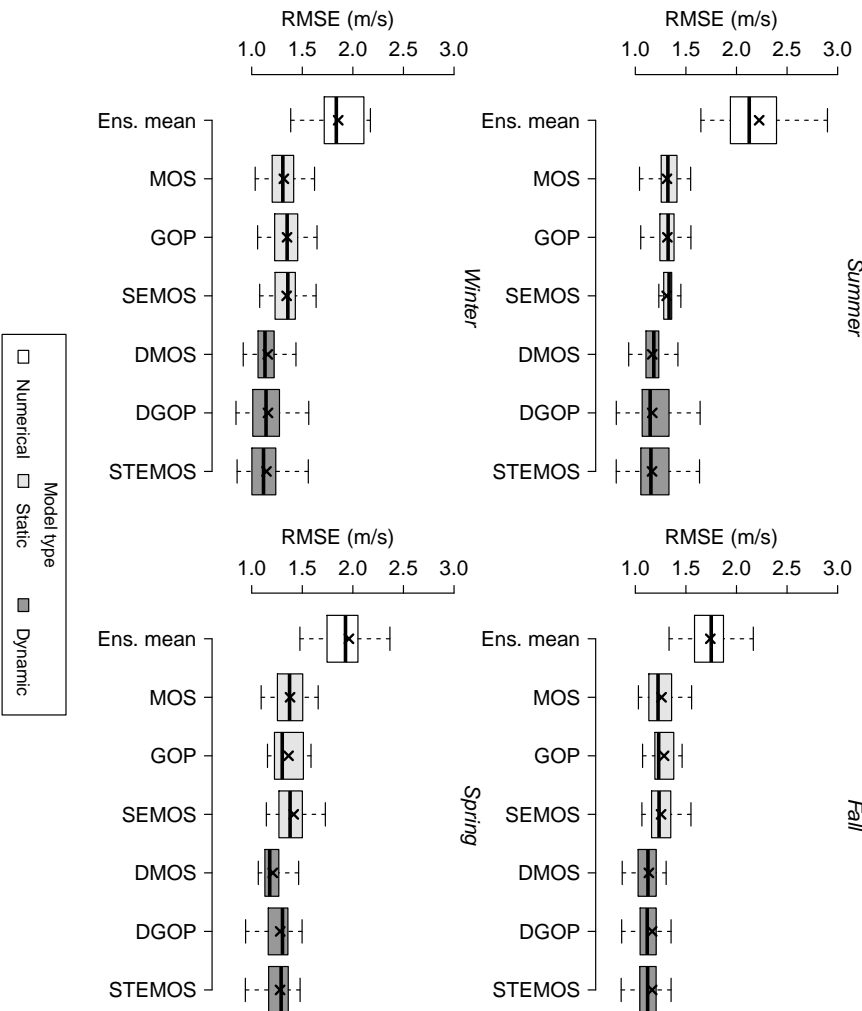


Figure 11: Boxplots of average RMSE of 24-h deterministic forecasts for wind speed at 10 meters over the seasons. The horizontal dense line and the \times symbol in each boxplot represent respectively, the median and the mean values.

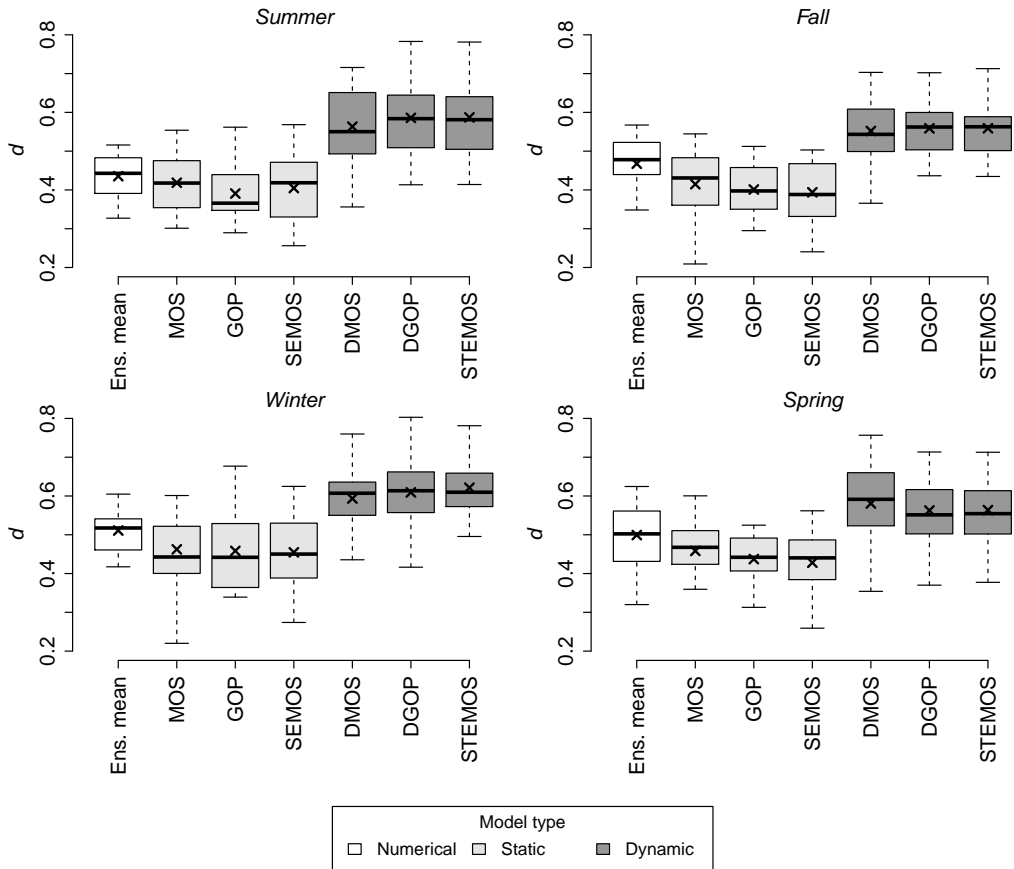


Figure 12: Boxplots of average index of agreement of 24-h deterministic forecasts for wind speed at 10 meters over the seasons. Absolute agreement between predictions and actual values occurs when $d = 1$. The horizontal dense line and the \times symbol in each boxplot represent respectively, the median and the mean values.

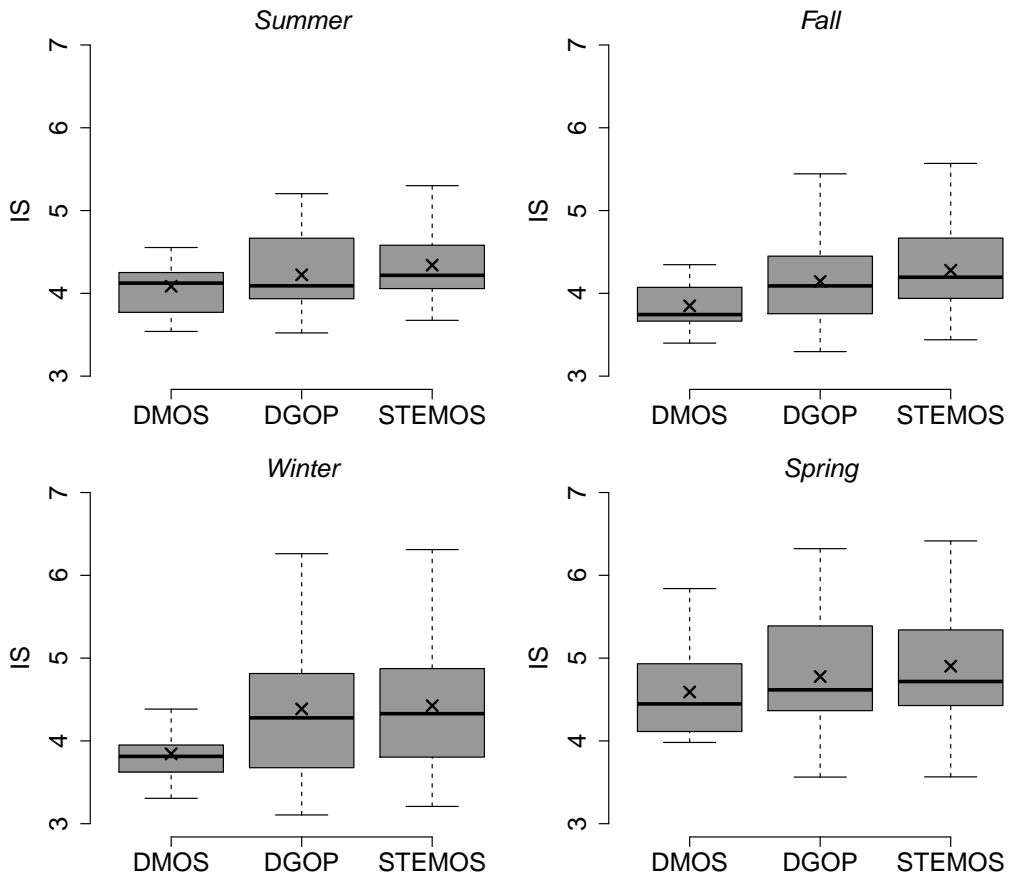


Figure 13: Boxplots of average IS of 24-h deterministic forecasts for wind speed at 10 meters over the seasons. The horizontal dense line and the \times symbol in each boxplot represent respectively, the median and the mean values.

References

Ailliot, P., Monbet, V., and Prevosto, M. “An autoregressive model with time-varying coefficients for wind fields.” *Environmetrics*, 17(2):107–117 (2006).

Amarante, O. d., Silva, F., and Andrade, P. “Atlas Eólico: Minas Gerais.” *Belo Horizonte: CEMIG* (2010).

Anderson, J. L. “A method for producing and evaluating probabilistic forecasts from ensemble model integrations.” *Journal of climate*, 9(7):1518–1530 (1996).

Bardossy, A. and Plate, E. J. “Space-time model for daily rainfall using atmospheric circulation patterns.” *Water Resources Research*, 28(5):1247–1259 (1992).

Black, T. L. “The new NMC mesoscale Eta model: Description and forecast examples.” *Weather and forecasting*, 9(2):265–278 (1994).

Box, G. E. and Cox, D. R. “An analysis of transformations.” *Journal of the Royal Statistical Society. Series B (Methodological)*, 211–252 (1964).

Carter, C. K. and Kohn, R. “On Gibbs sampling for state space models.” *Biometrika*, 81(3):541–553 (1994).

Chou, S., Souza, C. d., Gomes, J. L., Evangelista, E., Osório, C., and Cataldi, M. “Refinamento estatístico das previsões horárias de temperatura a 2 m do modelo Eta em estações do Nordeste do Brasil.” *Revista Brasileira de Meteorologia*, 22(3):287–296 (2007).

Cressie, N. *Statistics for spatial data*. New York: Wiley (1993).

Eddelbuettel, D., François, R., Allaire, J., Ushey, K., Kou, Q., Russel, N., Chambers, J., and Bates, D. “Rcpp: Seamless R and C++ integration.” *Journal of Statistical Software*, 40(8):1–18 (2011).

Epstein, E. S. “Stochastic dynamic prediction.” *Tellus*, 21(6):739–759 (1969).

Feldmann, K., Scheuerer, M., and Thorarinsdottir, T. L. “Spatial postprocessing of ensemble forecasts for temperature using nonhomogeneous Gaussian regression.” *Monthly Weather Review*, 143(3):955–971 (2015).

Frühwirth-Schnatter, S. “Data augmentation and dynamic linear models.” *Journal of time series analysis*, 15(2):183–202 (1994).

Gel, Y., Raftery, A. E., and Gneiting, T. “Calibrated probabilistic mesoscale weather field forecasting: The geostatistical output perturbation method.” *Journal of the American Statistical Association*, 99(467):575–583 (2004).

Gelman, A., Rubin, D. B., et al. “Inference from iterative simulation using multiple sequences.” *Statistical science*, 7(4):457–472 (1992).

Glahn, H. R. and Lowry, D. A. “The use of model output statistics (MOS) in objective weather forecasting.” *Journal of applied meteorology*, 11(8):1203–1211 (1972).

Gneiting, T. *Calibration of medium-range weather forecasts*. European Centre for Medium-Range Weather Forecasts (2014).

Gneiting, T. and Raftery, A. E. “Strictly proper scoring rules, prediction, and estimation.” *Journal of the American Statistical Association*, 102(477):359–378 (2007).

Gneiting, T., Raftery, A. E., Westveld III, A. H., and Goldman, T. “Calibrated probabilistic forecasting using ensemble model output statistics and minimum CRPS estimation.” *Monthly Weather Review*, 133(5):1098–1118 (2005).

Grimit, E. P. and Mass, C. F. “Measuring the ensemble spread–error relationship with a probabilistic approach: Stochastic ensemble results.” *Monthly weather review*, 135(1):203–221 (2007).

Hamill, T. M. “Interpretation of rank histograms for verifying ensemble forecasts.” *Monthly Weather Review*, 129(3):550–560 (2001).

Hansen, F. V. “Surface roughness lengths.” Technical Report ARL-TR-61, U.S. Army Research Laboratory (1993). 45p.

Kalman, R. E. “A new approach to linear filtering and prediction problems.” *Journal of basic Engineering*, 82(1):35–45 (1960).

Krishnamurti, T. “Numerical weather prediction.” *Annual review of fluid mechanics*, 27(1):195–225 (1995).

Lange, M. “On the uncertainty of wind power predictionsAnalysis of the forecast accuracy and statistical distribution of errors.” *Journal of solar energy engineering*, 127(2):177–184 (2005).

Li, W., Duan, Q., Miao, C., Ye, A., Gong, W., and Di, Z. “A review on statistical postprocessing methods for hydrometeorological ensemble forecasting.” *WIREs Water*, 4(e1246):1–24 (2017).

Mao, Q., McNider, R. T., Mueller, S. F., and Juang, H.-M. H. “An optimal model output calibration algorithm suitable for objective temperature forecasting.” *Weather and forecasting*, 14(2):190–202 (1999).

Matheson, J. E. and Winkler, R. L. “Scoring rules for continuous probability distributions.” *Management science*, 22(10):1087–1096 (1976).

Mesinger, F., Janjić, Z. I., Ničković, S., Gavrilov, D., and Deaven, D. G. “The step-mountain coordinate: model description and performance for cases of Alpine lee cyclogenesis and for a case of an Appalachian redevelopment.” *Monthly Weather Review*, 116(7):1493–1518 (1988).

Monin, A. S. and Obukhov, A. M. “Basic laws of turbulent mixing in the surface layer of the atmosphere.” *Contrib. Geophys. Inst. Acad. Sci. USSR*, 151(163):e187 (1954).

Piani, C., Haerter, J., and Coppola, E. “Statistical bias correction for daily precipitation in regional climate models over Europe.” *Theoretical and Applied Climatology*, 99(1-2):187–192 (2010).

R Core Team. *R: A Language and Environment for Statistical Computing*. R Foundation for Statistical Computing, Vienna, Austria (2017).
URL <http://www.R-project.org/>

Raftery, A. and Lewis, S. “The number of iterations, convergence diagnostics and generic Metropolis algorithms.” *Practical Markov Chain Monte Carlo* (1995).

Raftery, A. E., Gneiting, T., Balabdaoui, F., and Polakowski, M. “Using Bayesian model averaging to calibrate forecast ensembles.” *Monthly Weather Review*, 133(5):1155–1174 (2005).

Saha, S., Moorthi, S., Wu, X., Wang, J., Nadiga, S., Tripp, P., Behringer, D., Hou, Y.-T., Chuang, H.-y., Iredell, M., et al. “The NCEP climate forecast system version 2.” *Journal of Climate*, 27(6):2185–2208 (2014).

Sanderson, C. and Curtin, R. “Armadillo: a template-based C++ library for linear algebra.” *Journal of Open Source Software* (2016).

Sansó, B. and Guenni, L. “Venezuelan rainfall data analysed by using a Bayesian space–time model.” *Journal of the Royal Statistical Society: Series C (Applied Statistics)*, 48(3):345–362 (1999).

Scheuerer, M., Möller, D., et al. “Probabilistic wind speed forecasting on a grid based on ensemble model output statistics.” *The Annals of Applied Statistics*, 9(3):1328–1349 (2015).

Schuhen, N., Thorarinsdottir, T. L., and Gneiting, T. “Ensemble model output statistics for wind vectors.” *Monthly weather review*, 140(10):3204–3219 (2012).

Tanner, M. A. and Wong, W. H. “The calculation of posterior distributions by data augmentation.” *Journal of the American statistical Association*, 82(398):528–540 (1987).

Thorarinsdottir, T. L. and Gneiting, T. “Probabilistic forecasts of wind speed: ensemble model output statistics by using heteroscedastic censored regression.” *Journal of the Royal Statistical Society: Series A (Statistics in Society)*, 173(2):371–388 (2010).

Thorarinsdottir, T. L. and Johnson, M. S. “Probabilistic wind gust forecasting using nonhomogeneous Gaussian regression.” *Monthly Weather Review*, 140(3):889–897 (2012).

Vannitsem, S., Wilks, D., and Messner, J. *Statistical Postprocessing of Ensemble Forecasts*. Elsevier (2018).

Vihola, M. “Robust adaptive Metropolis algorithm with coerced acceptance rate.” *Statistics and Computing*, 22(5):997–1008 (2012).

West, M. and Harrison, P. *Bayesian forecasting and dynamic models*. 2nd ed. Springer Verlag, New York (1997).

Whitaker, J. S. and Loughe, A. F. “The relationship between ensemble spread and ensemble mean skill.” *Monthly weather review*, 126(12):3292–3302 (1998).

Willmott, C. J. “On the validation of models.” *Physical geography*, 2(2):184–194 (1981).

Wilson, L. J. and Vallée, M. “The Canadian updateable model output statistics (UMOS) system: Design and development tests.” *Weather and forecasting*, 17(2):206–222 (2002).